

# Development of a Potential Fe<sub>2</sub>O<sub>3</sub>-Based Photocatalyst Thin Film for Water Oxidation by Scanning Electrochemical Microscopy: Effects of Ag–Fe<sub>2</sub>O<sub>3</sub> Nanocomposite and Sn Doping

Jum Suk Jang, Ki Youl Yoon, Xiaoyin Xiao, Fu-Ren F. Fan, and Allen J. Bard\*

Center for Electrochemistry, Department of Chemistry and Biochemistry, University of Texas, Austin, Texas 78712

Received May 13, 2009. Revised Manuscript Received September 4, 2009

Ag–Fe<sub>2</sub>O<sub>3</sub> and Sn-doped Ag–Fe<sub>2</sub>O<sub>3</sub> nanocomposite photocatalysts were optimized by scanning photoelectrochemical microscopy (SPECM) as a potential photoelectrochemical material for visible light irradiation ( $\lambda \geq 420$  nm). The photocurrent vs potential response and the action spectra were investigated in a three-electrode cell. Among different mole ratios, the composition of nanocomposite with 50% Ag–50% Fe (atomic percentage) showed a dramatic improvement in photocurrent on a thin film electrode under visible light ( $\lambda \geq 420$  nm). The addition of 2 atomic % Sn (relative to Fe) produced an Ag–Fe<sub>2</sub>O<sub>3</sub> nanocomposite with the largest photocurrent in alkaline solution under visible light irradiation ( $\lambda \geq 420$  nm).

## 1. Introduction

A photoelectrochemical (PEC) system converts solar energy into chemical energy by producing fuels such as hydrogen gas from water.<sup>1,2</sup> While a great deal of progress has been made in our understanding of PEC systems, practical, inexpensive, efficient, and stable devices have not yet been developed. A PEC system utilizes a semiconductor electrode as the photoanode or photocathode. Among various materials,  $\alpha$ -Fe<sub>2</sub>O<sub>3</sub> has been considered to be a potential candidate for the PEC system because of its good stability, absorption in the visible region, and low cost.<sup>3,4</sup> Although  $\alpha$ -Fe<sub>2</sub>O<sub>3</sub> absorbs and utilizes about 40% of the incident solar spectra because of its small bandgap (approximately 2.2 eV),<sup>3–5</sup> its low conductivity and short hole diffusion length, which result in the rapid nonradiative electron–hole recombination inside the semiconductor, lead to low efficiencies in PEC systems.<sup>6–8</sup> There have been numerous attempts to improve the PEC properties of  $\alpha$ -Fe<sub>2</sub>O<sub>3</sub> by fabricating composites and adding noble metals as well as doping various

metallic cations.<sup>4,9–14</sup> Among various modification methods of the photocatalyst, loading with noble metal nanoparticles, such as Pt, Pd, Au, and Ag, has been utilized to enhance the photocatalytic activity of powders and thin films by suppressing the recombination and promoting the charge-transfer process of photogenerated electrons and holes at the photocatalyst/electrolyte interface.<sup>15–19</sup> Among these noble metal catalysts, Ag ion and Ag nanoparticles have played an important role in photocatalytic or PEC oxidation and also in water splitting reactions.<sup>20–23</sup> Watanabe and co-workers reported that 6 mol % Ag and Au nanoparticles deposited on the surface of Fe<sub>2</sub>O<sub>3</sub> enhanced the photocurrent under intense irradiation, because the surface metal nanoparticles promoted hole transfer from the valence band to the electrolyte, preventing recombination of the photogenerated electrons and holes. However, only a small amount of noble metal was loaded on the photocatalyst

\*Corresponding author. Tel: 512-471-3761. Fax: 512-471-0088. E-mail: ajbard@mail.utexas.edu.

- (1) Bard, A. J.; Fox, M. A. *Acc. Chem. Res.* **1995**, *28*, 141.
- (2) Park, J. H.; Kim, S.; Bard, A. J. *Nano Lett.* **2006**, *6*, 24.
- (3) Hardee, K. L.; Bard, A. J. *J. Electrochem. Soc.* **1976**, *123*, 1024.
- (4) Anderman, M.; Kennedy, J. H. In *Semiconductor Electrodes*, Finklea, H. O., Ed.; Elsevier: Amsterdam, 1988; Chapter 3.
- (5) Aroutiounian, V. M.; Arakelyan, V. M.; Shahnazaryan, G. E.; Hovhannisyan, H. R.; Wang, H.; Turner, J. A. *Solar Energy* **2007**, *81*, 1369.
- (6) Leland, J. K.; Bard, A. J. *J. Phys. Chem.* **1987**, *91*, 5076.
- (7) Kennedy, J. H.; Frese, K. W. Jr. *J. Electrochem. Soc.* **1978**, *125*, 709.
- (8) Dare-Edwards, M.; Goodenough, J. B.; Hamnett, A.; Trelvelick, P. R. *J. Chem. Soc., Faraday Trans. 1* **1983**, *79*, 2027.
- (9) Kay, A.; Cesar, I.; Grätzel, M. *J. Am. Chem. Soc.* **2006**, *128*, 15714.
- (10) Duret, A.; Grätzel, M. *J. Phys. Chem. B* **2005**, *109*, 17184.
- (11) Sartoretti, C. J.; Alexander, B. D.; Solarska, R.; Rutkowska, I. A.; Augustynski, J.; Cerny, R. *J. Phys. Chem. B* **2005**, *109*, 13685.

- (12) Glasscock, J. A.; Barnes, P. R. F.; Plumb, I. C.; Savvides, N. *J. Phys. Chem. C* **2007**, *111*, 16477.
- (13) Hu, Y. S.; Kleiman, S. A.; Forman, A. J.; Hazen, D.; Park, J. N.; McFarland, E. W. *Chem. Mater.* **2008**, *20*, 3803.
- (14) Ingler, W. B. Jr.; Baltrus, J. P.; Khan, S. U. M. *J. Am. Chem. Soc.* **2004**, *126*, 10238.
- (15) Watanabe, A.; Kozuka, H. *J. Phys. Chem. B* **2003**, *107*, 12713.
- (16) Pan, F.; Zhang, J.; Zhang, W.; Wang, T. M.; Cai, C. *Appl. Phys. Lett.* **2007**, *90*, 122114.
- (17) Cai, C.; Zhang, J.; Pan, F.; Zhang, W.; Zhu, H.; Wang, T. *Catal. Lett.* **2008**, *123*, 51.
- (18) Yang, J.; Li, D.; Zhang, Z.; Li, Q.; Wang, H. *J. Photochem. Photobiol., A* **2000**, *137*, 197.
- (19) Mohapatra, S. K.; Kondamudi, N.; Banerjee, S.; Misra, M. *Langmuir* **2008**, *24*, 11276.
- (20) Schurch, D.; Currao, A.; Sarkar, S.; Hodes, G.; Calzaferri, G. *J. Phys. Chem. B* **2002**, *106*, 12764.
- (21) Glaus, S.; Calzaferri, G.; Hoffmann, R. *Chem.—Eur. J.* **2002**, *8*, 1785.
- (22) Currao, A.; Reddy, V. R.; Veen, M. K.; Schropp, R. E. I.; Calzaferri, G. *Photochem. Photobiol. Sci.* **2004**, *3*, 1017–1025.
- (23) Zhao, G.; Kozuka, H.; Yoko, T. *Thin Solid Films* **1996**, *277*, 147.

to improve its photocatalytic activity to minimize the absorption of incident light by the metal nanoparticles and their roles as recombination centers for photogenerated electrons.<sup>14</sup> Pan et al. reported that a Ag microgrid-connected TiO<sub>2</sub> nanocrystalline film enhanced the photocatalytic decomposition of methylene blue, where clearly the amount of Ag far exceeded the traditional loading of a few percent.<sup>15,16</sup>

Recently our group has reported a scanning photoelectrochemical microscopy (SPECM) technique for rapid screening of photocatalysts.<sup>24</sup> The technique is based on SECM in which the light through an optical fiber is used to illuminate individual spots on a photocatalyst array. The photocurrent recorded at each spot thus represents the activity of the photocatalyst, each with a different composition or structure, and it has recently been applied to doped Fe<sub>2</sub>O<sub>3</sub>-based photocatalysts.<sup>25</sup>

In the present work, unlike previously reported results, we investigated with SPECM that the content of Ag exceeded the usual amount for improvement of the Fe<sub>2</sub>O<sub>3</sub> photocatalyst because of the extraordinary morphology of the Ag-Fe<sub>2</sub>O<sub>3</sub> nanocomposite. We screened the atomic ratio of Ag to Fe in an Ag-Fe<sub>2</sub>O<sub>3</sub> nanocomposite photocatalyst and also investigated the doping effect of Sn in the Ag-Fe<sub>2</sub>O<sub>3</sub> nanocomposites. We used SPECM to obtain the photoresponse of these nanocomposites for water oxidation in 0.2 M NaOH solution under visible light irradiation ( $\lambda \geq 420$  nm). The PEC properties of the best compositions of bulk Ag-Fe<sub>2</sub>O<sub>3</sub> and Sn doped Ag-Fe<sub>2</sub>O<sub>3</sub> nanocomposites were also investigated.

## 2. Experimental Section

**2.1. Materials.** F-doped tin oxide (FTO) coated glass was obtained from Pilkington (Toledo, OH). 15 mm  $\times$  15 mm squares were cleaned by sonicating successively in ethanol and isopropanol and rinsed with deionized water. Fe(NO<sub>3</sub>)<sub>3</sub>·9H<sub>2</sub>O (Aldrich), AgNO<sub>3</sub> (Aldrich), Sn(C<sub>2</sub>H<sub>3</sub>O<sub>2</sub>)<sub>4</sub> (Aldrich), and ethylene glycol (Fisher) were used as received. All metal precursor solutions were made with ethylene glycol (EG) with a metal-salt concentration of 0.2 and 0.04 M.

**2.2. Preparation of Photocatalyst Spot Arrays.** A CH Instruments model 1550 Dispenser (Austin, TX) was used to fabricate the photocatalyst arrays. The model 1550 consists of a step motor operated at the XYZ stage with a piezo-dispenser (MicroJet AB-01-60, MicroFab, Plano, TX) attached to the head. The system was connected and controlled through a PC computer. The substrate (FTO) was placed underneath the piezo-dispenser tip. The XYZ stage moved the dispenser head in a preprogrammed pattern, while a voltage pulse was applied to the piezo-dispenser to eject various numbers of  $\sim$ 100 pL drops of the metal precursor solution onto the substrate. The first component (metal precursor solution) was loaded and dispensed in a preprogrammed pattern onto FTO substrate. After flushing and washing the piezo-dispenser, the second component was loaded into the dispenser and dispensed into an overlying pattern. The step was repeated when a third

component was added. The Ag-Fe and Ag-Sn/Fe spot arrays were calcined at 500 °C for 3 h.

**2.3. Screening the Spot Arrays.** A schematic of the SPECM setup was shown in our previous paper.<sup>23</sup> An optical fiber (FT-400-URT, 3M, St. Paul, MN) connected to a 150 W xenon lamp was attached to the tip holder of a CHI model 900B SECM. The array was placed in a SECM cell made of Teflon with the FTO/photocatalyst working electrode array exposed at the bottom through an O-ring. A Pt-gauze and an Ag/AgCl electrode were used as counter and reference electrodes, and a 0.2 M NaOH solution was used as the electrolyte. Light from a 150 W xenon lamp was passed through the optical fiber, which was positioned perpendicular to the working electrode surface and illuminated onto the working electrode. The optical fiber tip was held and scanned 50  $\mu$ m above the working electrode surface, while a potential bias was applied to the working electrode array. The photocurrent produced during the scan was recorded and displayed into a two-dimensional image. The applied potential was 0.2 V vs Ag/AgCl.

**2.4. Preparation and Photocurrent Measurement of Ag-Fe<sub>2</sub>O<sub>3</sub> and Ag-Fe<sub>2</sub>O<sub>3</sub>(2%Sn) Thin Film Electrodes.** Solutions containing 50% Ag-50% Fe (notated as Ag-Fe<sub>2</sub>O<sub>3</sub>) and Ag-Fe (1:1) with 2% Sn dopant (mole % to Fe) (denoted as Ag-Fe<sub>2</sub>O<sub>3</sub>(2%Sn)) compositions were prepared in ethylene glycol. The solutions were spin coated on cleaned FTO coated glass substrates at 2600 rpm for 20 s followed by drying at 500 °C for 10 min in air after each coating, and this process was repeated 5 times. Finally, the samples were calcined at 500 °C for 3 h. The electrochemical cell was a three electrode cell with a thin film electrode (0.18 cm<sup>2</sup>), Ag/AgCl and Pt gauze as photoanode, and reference and counter electrodes, respectively. The photoanode was illuminated with a Xe lamp (150 W) equipped with a UV cutoff filter ( $\lambda \geq 420$  nm). The photocurrent vs potential ( $I-V$ ) was measured in 0.2 M NaOH solution under UV or visible light condition ( $\lambda \geq 420$  nm). The chronoamperometry curves of the thin film electrode were also obtained at 0.4 V vs Ag/AgCl in the dark or under illumination.

**2.5. Physico-Chemical Characterization.** X-ray Diffraction (XRD) measurements were carried out using a Bruker-Norius D8 advanced diffractometer. The Cu K radiation source was operated at 40 kV and 40 mA. All measurements were carried out in the ( $\theta/2\theta$ ) mode. Samples for XRD analysis were prepared using the same metal salt solution used to fabricate the photocatalyst arrays. The optical properties of the undoped and doped iron oxide films were obtained with a UV-visible diffuse reflectance spectrophotometer (Milton Roy Spectronic 3000 Array). The solutions were mixed in 25 mL vials with the optimum ratio determined by SPECM experiments and were then heated at 500 °C for 3 h. The powers obtained were used for SEM, TEM, and XRD analyses.

## 3. Results and Discussion

To develop iron oxide (Fe<sub>2</sub>O<sub>3</sub>) based photocatalysts that are photoactive under visible light irradiation, we applied SPECM, which has been used to screen doping with various metal cations (Ni, Eu, Co) and noble metals (Pt, Pd) in our previous studies.<sup>24,25</sup>

**3.1. SPECM Studies on the Ag-Fe Composite System.** In this study, spot arrays of Ag-Fe composites with different concentrations of Ag precursor (0-100% dopant in 10% increments) were fabricated and screened by SPECM. The array was prepared from a solution of 0.2 M Fe(NO<sub>3</sub>)<sub>3</sub>·9H<sub>2</sub>O and 0.2 M AgNO<sub>3</sub> in ethylene glycol

(24) Lee, J.; Ye, H.; Pan, S.; Bard, A. J. *Anal. Chem.* **2008**, *80*, 7445.

(25) Jang, J. S.; Lee, J.; Ye, H.; Fan, F.-R.; Bard, A. J. *J. Phys. Chem. C* **2009**, *113*(16), 6719.

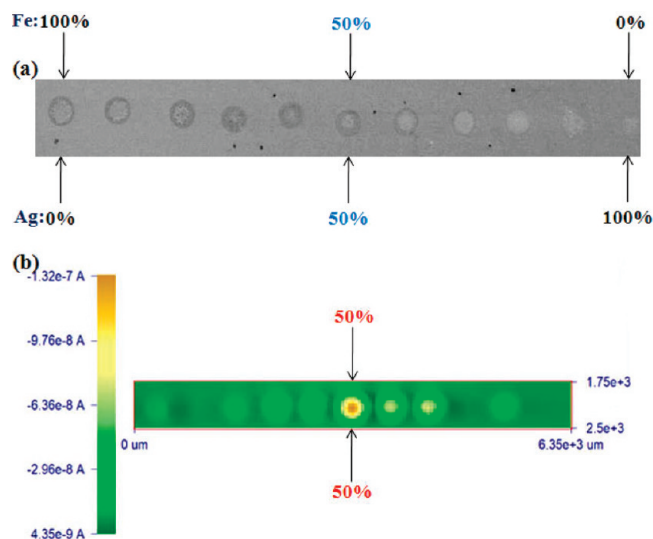


**Figure 1.** (a) Optical image of dispensed pattern of spots showing atomic ratios of Ag to Fe in the row. (b) SPCM image one line of a spot array at applied potential of 0.2 V vs Ag/AgCl in 0.2 M NaOH under visible light irradiation ( $\lambda \geq 420$  nm).

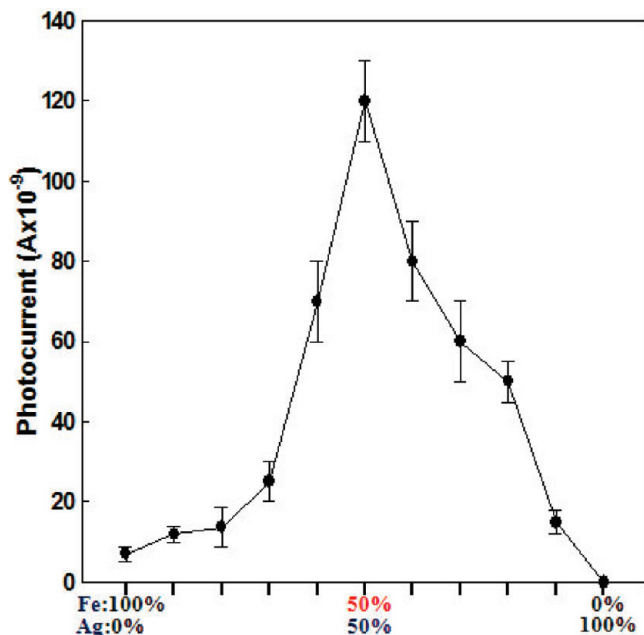


**Figure 2.** Dependence of photocurrent of the spot array on atomic ratio of Ag to Fe. All photocurrents were obtained from three lines of spots in Figure 1b.

(EG). As shown in Figure 1a, the 1st to 10th spots in a row represent compositions from 100%  $\text{Fe}_2\text{O}_3$  (10 drops of  $\text{Fe}(\text{NO}_3)_3$ ) to 100% Ag metal (10 drops of  $\text{AgNO}_3$ ) with 10% changes for each successive drop. Figure 1b shows the SPCM image obtained from these spots. Note that the composition with 50% Ag–50% Fe showed the highest photocurrent under visible light ( $\lambda \geq 420$  nm) irradiation at 0.2 V vs Ag/AgCl (0.4 V vs NHE). As shown in Figure 2 of the photocurrent as a function of composition obtained from the SPCM image, addition of Ag produces a significant increase in the photocurrent, with a maximum at the atomic ratio of 1:1 Ag–Fe about 17 times higher than that of a pure  $\text{Fe}_2\text{O}_3$  spot. Increasing

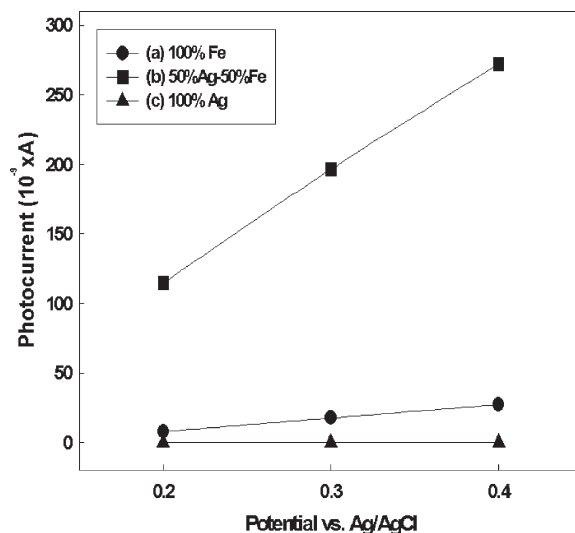


**Figure 3.** Dependence of photocurrent of Ag–Fe spot array on the applied potential (0.2, 0.3, and 0.4 V). (Circles, a): 100% Fe, (squares, b): 50% Ag–50% Fe, (triangles, c): 100% Ag. Electrolyte solution: 0.2 M NaOH, light source: 150 W Xe lamp.

the atomic ratio of Ag to Fe above this value produced a decrease in efficiency, partially due to the decrease in photoactive material ( $\text{Fe}_2\text{O}_3$ ) inside the photocatalyst spot and partially due to the light-blocking effect of a high loading of Ag on the light absorption of the  $\text{Fe}_2\text{O}_3$ .<sup>26,27</sup> As shown below, the Ag exists in these films as metallic Ag, so higher loading of Ag may also create recombination centers within the bandgap.

The SPCM images obtained from the same array at different potentials, such as 0.3 and 0.4 V vs Ag/AgCl, show similar trends in the photocurrent (see Figure S1 in the Supporting Information). Figure 3 shows the photocurrents as a function of applied potential (0.2, 0.3, and 0.4 V) from the SPCM images. The photocurrents of  $\text{Fe}_2\text{O}_3$  and 50% Ag–50% Fe spots increased linearly with the increase of applied potential in this region.

**3.2. SPCM Studies on the Effect of Tin Doping.** Several research groups<sup>6–8</sup> have reported that the photocurrent of  $\text{Fe}_2\text{O}_3$  can be enhanced by doping with elements with a 4+ oxidation state such as  $\text{Sn}^{+4}$ ,  $\text{Ti}^{+4}$ , and  $\text{Si}^{+4}$ . To improve the PEC activity of Ag– $\text{Fe}_2\text{O}_3$  nanocomposites we investigated the effect of adding Sn as a dopant to Ag– $\text{Fe}_2\text{O}_3$ .  $\text{Sn}^{+4}$  can substitute for  $\text{Fe}^{+3}$  in the hematite lattice. After reducing  $\text{Sn}^{+4}$  to  $\text{Sn}^{+2}$  by thermal treatment in the presence of a reducing agent (e.g., EG), it can act as an electron donor which can improve the electrical conductivity of  $\text{Fe}_2\text{O}_3$ . To investigate the optimal concentration of Sn in the Ag– $\text{Fe}_2\text{O}_3$  nanocomposite, we fixed the atomic ratio as 1:1 Ag–Fe and changed the amount of tin dopant up to 10% of the Fe (0 to 10% dopant in 2% increment).

For the screening of Sn dopant on Ag–Fe nanocomposite photocatalyst the array pattern was prepared from a mixed solution of 0.2 M  $\text{AgNO}_3$  and  $\text{Fe}(\text{NO}_3)_3$  with

(26) Subramanian, V.; Wolf, E.; Kamat, P. V. *J. Phys. Chem. B* **2001**, *105*, 11439.

(27) Shan, Z.; Wu, J.; Xu, F.; Huang, F.; Ding, H. *J. Phys. Chem. C* **2008**, *112*, 15423.

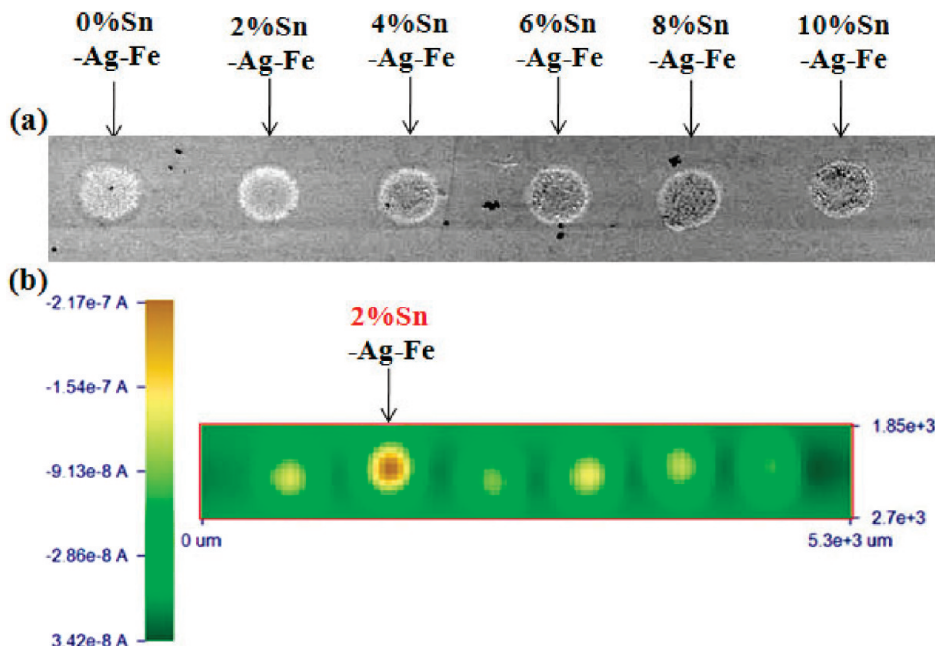


**Figure 4.** (a) Dispensed pattern of spot array with different doping atom % of Sn to Fe in (1:1) Ag-Fe. (b) SPCM image measured with spot arrays at applied potential of 0.2 V vs Ag/AgCl in 0.2 M NaOH under visible light irradiation ( $\lambda \geq 420$  nm).

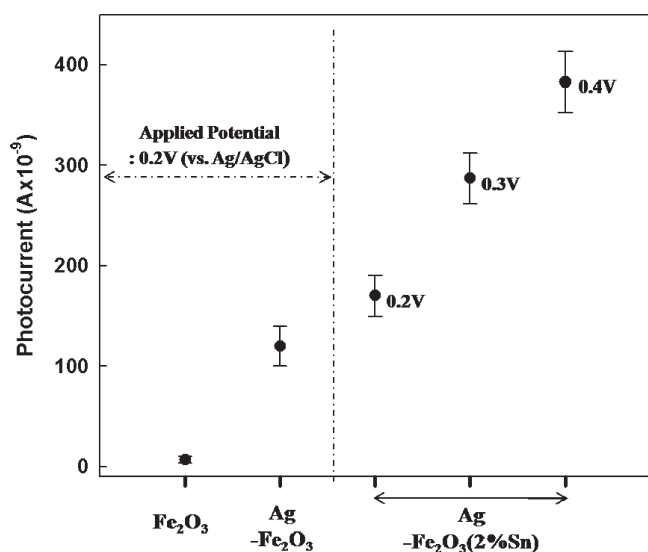


**Figure 5.** Photocurrents of (a) Fe<sub>2</sub>O<sub>3</sub>, (b) Ag-Fe<sub>2</sub>O<sub>3</sub>, (c) Ag-Fe<sub>2</sub>O<sub>3</sub>(2% Sn) obtained from SPCM spot array. Electrolyte solution: 0.2 M NaOH, light source: 150 W Xe lamp, applied potential: 0.2 V vs Ag/AgCl. Photocurrents of 2% Sn spot were obtained at applied potentials of 0.2, 0.3, and 0.4 V.

additions of 0.04 M Sn(C<sub>2</sub>H<sub>3</sub>O<sub>2</sub>)<sub>4</sub> resulting in spots with compositions shown in Figure 4a. The first and sixth spots in a row were 50% Ag-50% Fe and 50% Ag-50% Fe with 10% Sn (atom % to Fe), respectively. Figure 4b shows the result of SPCM image obtained from this photocatalyst spot array. A maximum photocurrent (170 nA) was observed at the composition with 2% Sn in the Ag-Fe spot, which was ~1.4 times larger than that of 1:1 Ag-Fe<sub>2</sub>O<sub>3</sub> (120 nA), but decreased gradually with a further increase of the amount of Sn. Figure 5 summarizes the photocurrents obtained under visible light irradiation ( $\lambda \geq 420$  nm) and the potential dependence with the 2% Sn spot.

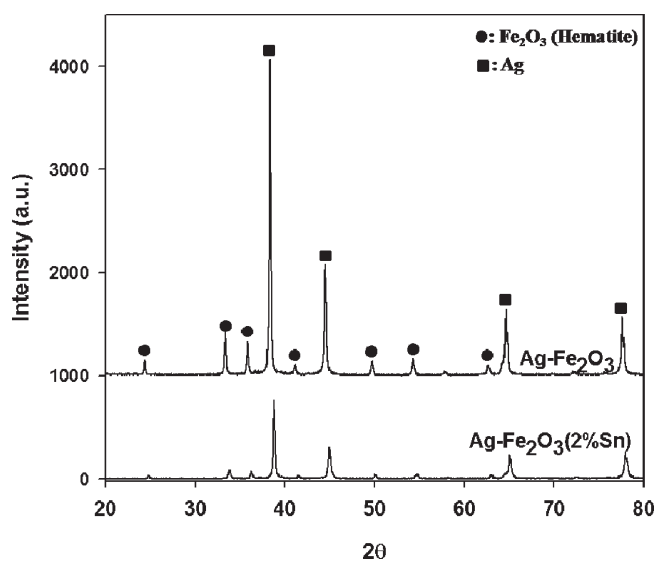


**Figure 6.** XRD patterns of (a) Ag-Fe<sub>2</sub>O<sub>3</sub> and (b) Ag-Fe<sub>2</sub>O<sub>3</sub>(2%Sn) samples.

**3.3. Physicochemical Characterization of Nanocomposite Samples.** Figure 6 shows the XRD patterns of Ag-Fe<sub>2</sub>O<sub>3</sub> and Ag-Fe<sub>2</sub>O<sub>3</sub>(2%Sn) samples. These samples, formed via pyrolysis of the mixture solution containing iron(III) nitrate solution and silver nitrate and tin acetate as dopant, show patterns for metallic Ag and α-Fe<sub>2</sub>O<sub>3</sub> (hematite), indicating the absence of other impurity phases, even with Sn doping of Fe<sub>2</sub>O<sub>3</sub> and Ag and the high temperature calcination process.

Optical properties of the Ag-Fe<sub>2</sub>O<sub>3</sub> and Ag-Fe<sub>2</sub>O<sub>3</sub>(2%Sn) thin films were measured by UV-visible absorption spectra as shown in Figure 7. Both samples showed an absorption peak at around 590 nm (2.1 eV), a shoulder around 540 nm (2.3 eV), and at peak around 400 nm (3.1 eV). Note that two absorbances at short wavelengths are

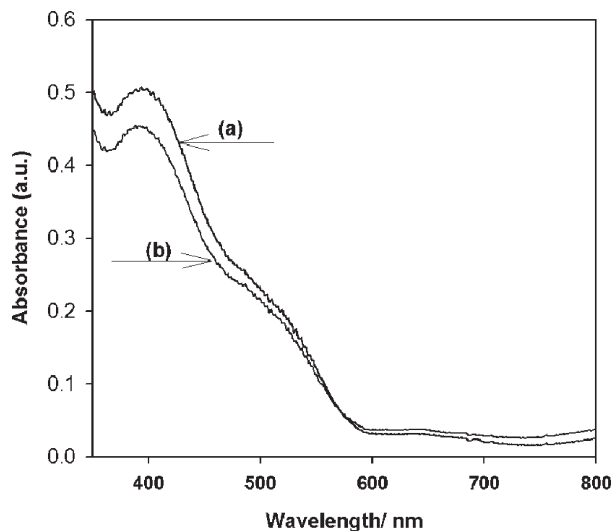


**Figure 7.** UV-visible spectra of (a) Ag-Fe<sub>2</sub>O<sub>3</sub> and (b) Ag-Fe<sub>2</sub>O<sub>3</sub>(2%Sn) thin films.

much stronger, reflecting the selection rules. The absorption spectra of the two samples are very similar to that of a pure  $\alpha$ -Fe<sub>2</sub>O<sub>3</sub> thin film.<sup>9</sup>

The morphologies of the Ag-Fe<sub>2</sub>O<sub>3</sub> and Ag-Fe<sub>2</sub>O<sub>3</sub>(2%Sn) films determined by SEM are shown in Figure 8. In both samples, large particles of approximately 0.5–1  $\mu$ m were decorated with small nanoparticles of approximately 100 nm. To obtain a better idea of the structures and the location of the Fe<sub>2</sub>O<sub>3</sub> and Ag metal in the nanocomposites, we obtained TEM images (Figure 9) (see Figure S2 in the Supporting Information for TEM-EDAX spectrum). We find the larger particles with sizes of approximately 0.5–1  $\mu$ m were Ag metal and the smaller particles with sizes of approximately 60–70 nm were Fe<sub>2</sub>O<sub>3</sub>. In addition, there were small Ag particles, approximately 5 nm, on the surface of Fe<sub>2</sub>O<sub>3</sub>. These Ag particles were confirmed by EDS analysis. The proposed structure of the Ag-Fe<sub>2</sub>O<sub>3</sub> nanocomposite then at this stage is Ag particles of approximately 0.5–1  $\mu$ m decorated with Fe<sub>2</sub>O<sub>3</sub> nanoparticles of approximately 60–70 nm, with Ag metal nanoparticles of approximately 5 nm attached on the Fe<sub>2</sub>O<sub>3</sub> nanoparticle surface. A cartoon showing this proposed structure is shown in Figure 9b. Note that Fe<sub>2</sub>O<sub>3</sub> particles would form random multiple particle layers on the surface of a large Ag metal particle, and Ag nanoparticles are well dispersed on the surface of Fe<sub>2</sub>O<sub>3</sub>. This configuration perhaps favors an effective separation of photogenerated electrons and holes and thus increases the PEC properties of nanocomposite materials such as those reported for other composite photocatalysts,<sup>22,28,29</sup> even with high amount of Ag metal loading.

**3.4. PEC Effects on Bulk Thin Film Electrodes—Comparison with SPECM Study.** To confirm the correlation between SPECM results and bulk films, we measured the photocurrents of Ag-Fe<sub>2</sub>O<sub>3</sub> and Ag-Fe<sub>2</sub>O<sub>3</sub>(2%Sn) film

electrodes coated on FTO glass under visible light ( $\lambda \geq 420$  nm). The PEC measurements were performed in a glass cell to facilitate the transmittance of light to the photoelectrode surface and illuminated with a xenon lamp (150 mW/cm<sup>2</sup>). The working electrode had a surface area of 0.18 cm<sup>2</sup>, and a Pt gauze and an Ag/AgCl electrode were used as the counter and reference electrodes, respectively. The electrolyte solution used for all measurements was 0.2 M NaOH.

As seen in Figure 10, an Ag-Fe<sub>2</sub>O<sub>3</sub>(2%Sn) film electrode showed a higher photocurrent than that of Ag-Fe<sub>2</sub>O<sub>3</sub> over the potential range of 0.1 to 0.5 V vs Ag/AgCl (0.3 to 0.7 V vs NHE) in 0.2 M NaOH solution. Note that the on-set potential of the anodic photocurrent is about 0.05 V vs Ag/AgCl, which is about 0.2 V negative of the thermodynamic potential for water oxidation in 0.2 M NaOH. The anodic photocurrents of Ag-Fe<sub>2</sub>O<sub>3</sub> and Ag-Fe<sub>2</sub>O<sub>3</sub>(2%Sn) electrodes are approximately 58 and 366  $\mu$ A/cm<sup>2</sup> at a bias of 0.4 V vs Ag/AgCl under visible light ( $\lambda \geq 420$  nm) irradiation, respectively. Figure 11 shows the chopped current-time transient responses of Ag-Fe<sub>2</sub>O<sub>3</sub> and Ag-Fe<sub>2</sub>O<sub>3</sub>(2%Sn) thin film electrodes under visible ( $\lambda \geq 420$  nm) and UV irradiation. The Ag-Fe<sub>2</sub>O<sub>3</sub>(2%Sn) thin film showed a good photosensitivity under UV and visible light irradiation, that is, a high photocurrent under illumination relative to the dark current and also good photostability in an alkaline solution (see Figure S3 in the Supporting Information). The photocurrent of the Ag-Fe<sub>2</sub>O<sub>3</sub>(2%Sn) thin film is about 6 times that of Ag-Fe<sub>2</sub>O<sub>3</sub> thin film under visible and UV light irradiation, respectively.

In general, pure Fe<sub>2</sub>O<sub>3</sub> is an insulator at room temperature with a specific resistance of approximately 10<sup>12</sup>  $\Omega$  cm.<sup>4</sup> We examined the resistance of our films coated on glass in the air at room temperature under dark conditions (Figure 12). The  $I$ - $V$  curves of the Ag-Fe<sub>2</sub>O<sub>3</sub> and Ag-Fe<sub>2</sub>O<sub>3</sub>(2%Sn) thin films suggest that the resistance of Fe<sub>2</sub>O<sub>3</sub> decreased when formed as a nanocomposite with Ag and Sn. Thus the conductivities of these thin films were improved by Ag metal and Sn addition in a nanocomposite configuration.

The flat-band potentials,  $E_{fb}$ , of the Ag-Fe<sub>2</sub>O<sub>3</sub> and Ag-Fe<sub>2</sub>O<sub>3</sub>(2%Sn) thin film electrodes were measured via Mott-Schottky (M-S) plots of  $1/C_{sc}^2$  vs potentials (where  $C_{sc}$  is the space charge capacitance) in 0.2 M NaOH. Figure 13 shows the M-S plots for the Ag-Fe<sub>2</sub>O<sub>3</sub> and Ag-Fe<sub>2</sub>O<sub>3</sub>(2%Sn) thin film electrodes in 0.2 M NaOH. The value of  $E_{fb}$  shifted positively from approximately -0.37 to -0.2 V in this solution before and after doping with Sn.

To estimate the incident photon to current conversion efficiency (IPCE) of Ag-Fe<sub>2</sub>O<sub>3</sub>(2%Sn) thin film electrodes, we carried out monochromatic irradiation provided by a 150 W Xe lamp attached to a monochromator. The photocurrents were measured at each wavelength under potentiostatic control (0.3 or 0.4 V) (see Figure S4 in the Supporting Information). Figure 14 shows the IPCE as a function of wavelength. The IPCE of Ag-Fe<sub>2</sub>O<sub>3</sub>(2%Sn) obtained at 420 nm is 1.4 and 2.0% at 0.3 and 0.4 V

(28) Yu, J.; Xiong, J.; Cheng, B.; Liu, S. *Appl. Catal., B* **2005**, *60*, 211.  
 (29) Jang, J. S.; Lee, J. S.; Li, W.; Oh, S. H. *Chem. Phys. Lett.* **2006**, *425*, 278.

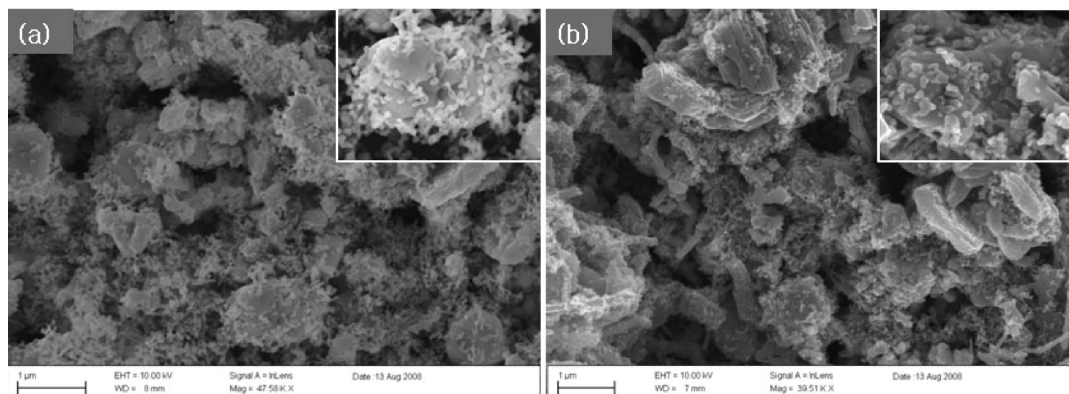


Figure 8. SEM images of (a) Ag-Fe<sub>2</sub>O<sub>3</sub> and (b) Ag-Fe<sub>2</sub>O<sub>3</sub>(2%Sn) samples.

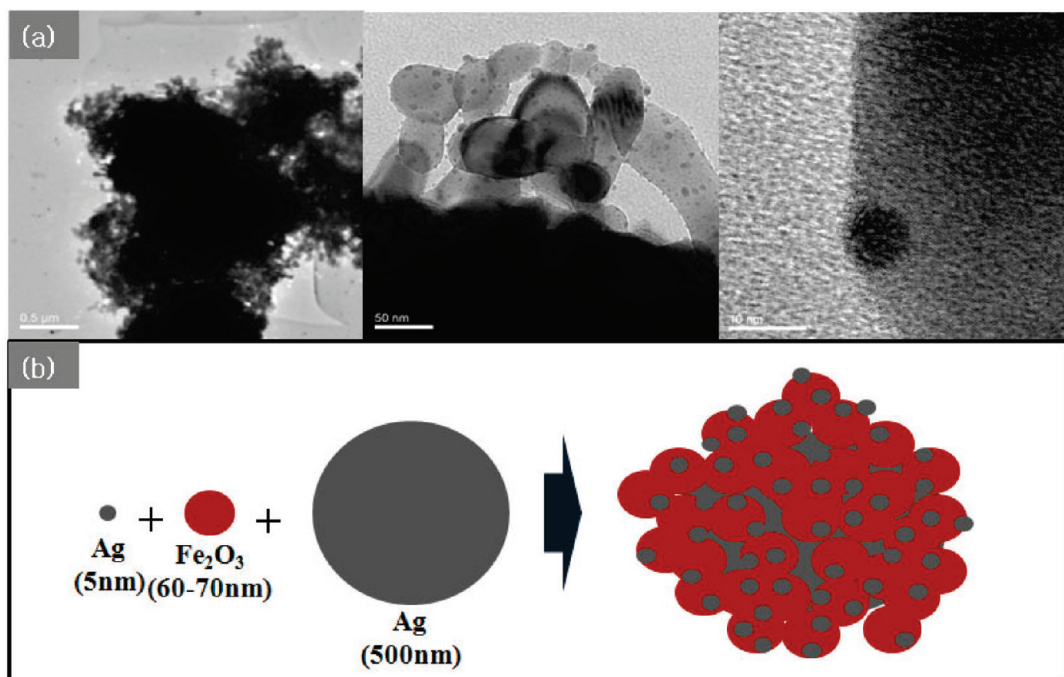


Figure 9. TEM images of (a) Ag-Fe<sub>2</sub>O<sub>3</sub> sample and (b) a cartoon of nanocomposite photocatalyst consisting of Ag and Fe<sub>2</sub>O<sub>3</sub> nanoparticles.

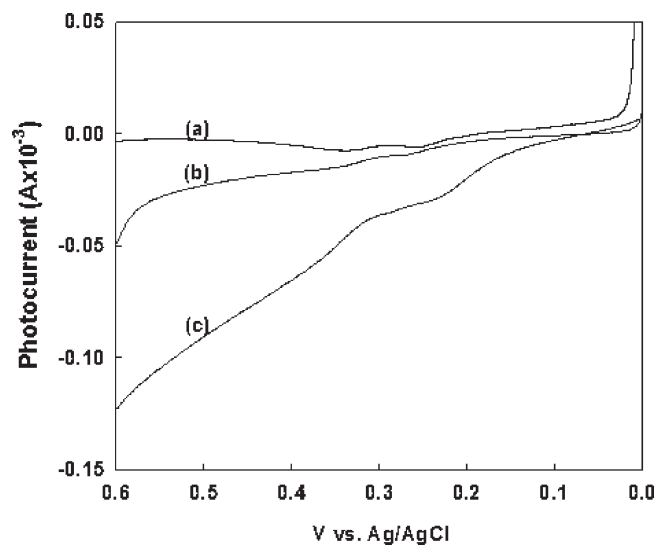


Figure 10. Photocurrent vs potential curves for (a) Ag-Fe<sub>2</sub>O<sub>3</sub> (dark) and (b) Ag-Fe<sub>2</sub>O<sub>3</sub> and (c) Ag-Fe<sub>2</sub>O<sub>3</sub>(2%Sn) thin film electrodes (0.18 cm<sup>2</sup>) under visible light irradiation ( $\lambda \geq 420$  nm). The sweep rate: 0.5 mV/s, electrolyte solution: 0.2 M NaOH, light source: 150 W Xe lamp.

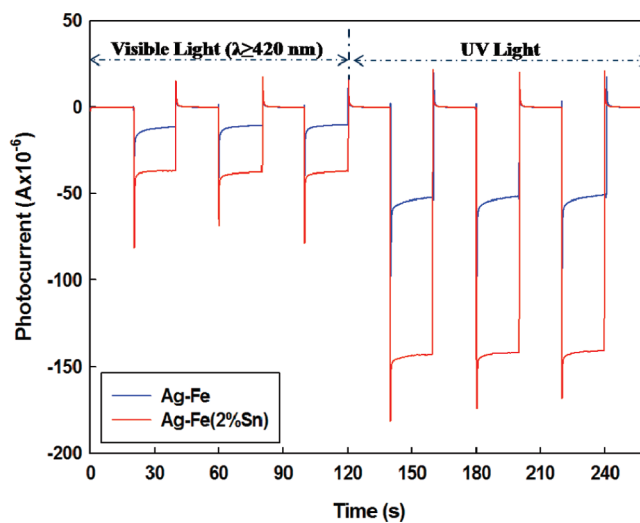
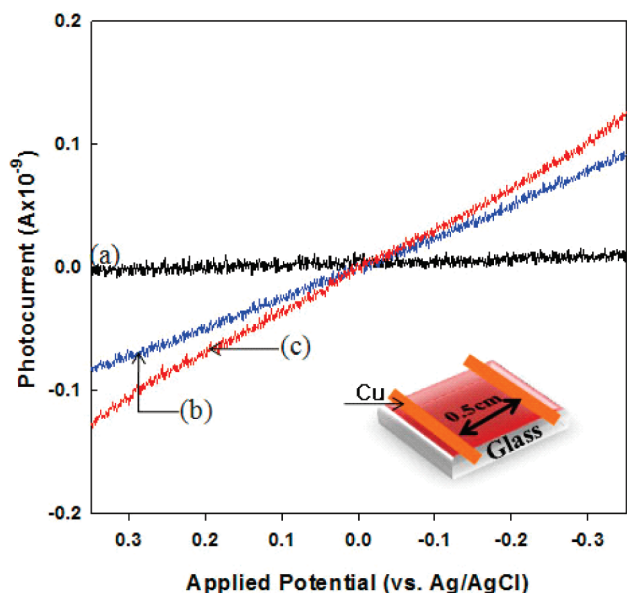
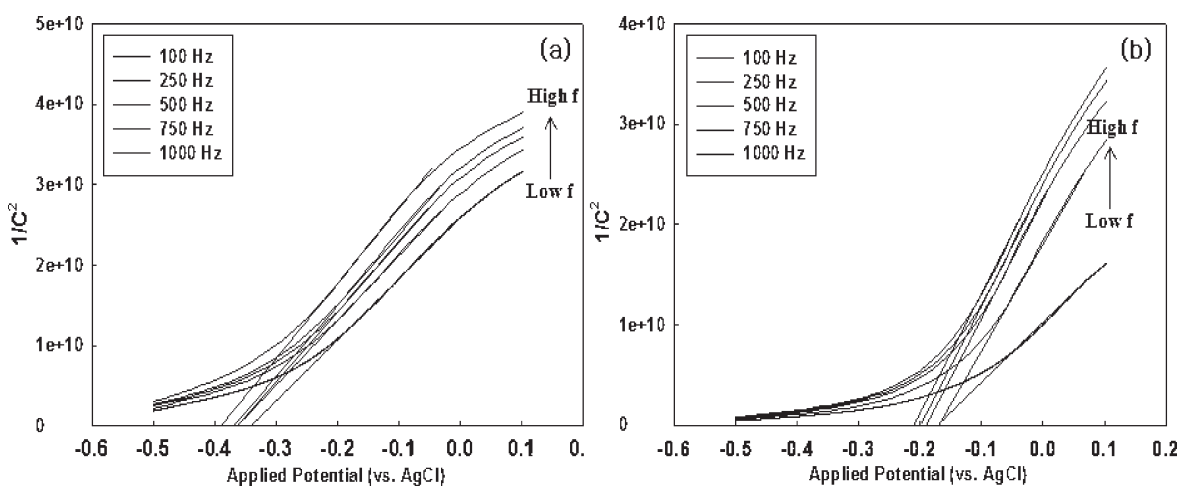


Figure 11. Chopped current-time transient response of (a) Ag-Fe<sub>2</sub>O<sub>3</sub>, (b) Ag-Fe<sub>2</sub>O<sub>3</sub>(2%Sn) thin film electrode under visible ( $\lambda \geq 420$  nm), and UV light irradiation. Electrolyte solution: 0.2 M NaOH, light source: 150 W Xe lamp, applied potential: 0.3 V vs Ag/AgCl.



**Figure 12.** Current–voltage curves in the dark across (a) a glass substrate, (b) an Ag–Fe<sub>2</sub>O<sub>3</sub> thin film, and (c) an Ag–Fe<sub>2</sub>O<sub>3</sub>(2%Sn) thin film coated on the glass substrate. The dimension of the Ag–Fe<sub>2</sub>O<sub>3</sub> and Ag–Fe<sub>2</sub>O<sub>3</sub>(2%Sn) thin films was 18 mm × 5 mm × ~450 nm (thickness).



**Figure 13.** Mott–Schottky plots of (a) Ag–Fe<sub>2</sub>O<sub>3</sub> and (b) Ag–Fe<sub>2</sub>O<sub>3</sub>(2%Sn) thin films in 0.2 M NaOH solution in the dark.

Ag/AgCl, respectively. The IPCE onsets of Ag–Fe<sub>2</sub>O<sub>3</sub> and Ag–Fe<sub>2</sub>O<sub>3</sub>(2%Sn) thin film electrodes generated above 600 nm, which agrees well with their absorption spectra<sup>7,8</sup> and the maximum value of IPCE, are seen around 375 nm. Note that the maximum power of light source measured with monochromator and power meter is obtained around 475 nm as shown in the inset of Figure 14. Thus, it could be considered that the photocurrent is mainly affected by the direct transitions from valence band orbitals to the conduction band edge ( $2p\text{ O}^{2-} \rightarrow 3d\text{ Fe}^{3+}$ , 257–413 nm) and not by the indirect  $d \rightarrow d$  type transition (at ~564 nm). Even though Ag–Fe<sub>2</sub>O<sub>3</sub> and Ag–Fe<sub>2</sub>O<sub>3</sub>(2%Sn) nanocomposite configuration improves the photocatalytic efficiency, the IPCE is still below 2% at low bias. However, the present work demonstrates an effective strategy for improving Fe<sub>2</sub>O<sub>3</sub>-based photocatalysts that might be applicable to other materials.

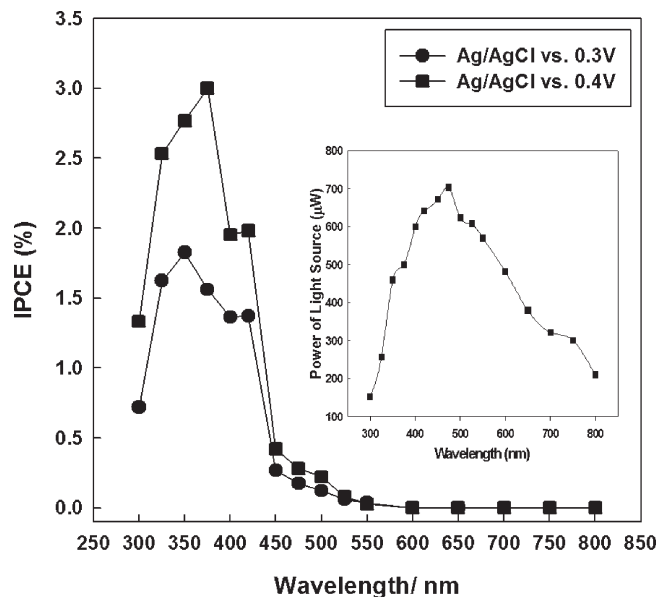


**Figure 14.** IPCE curve of Ag–Fe<sub>2</sub>O<sub>3</sub>(2%Sn) thin film electrode. Electrolyte solution: 0.2 M NaOH, light source: 150 W Xe lamp, applied potential: 0.3 or 0.4 V vs Ag/AgCl. The inset figure indicates the power of the lamp at different wavelengths.

Finally, we rationalize how the nanocomposite configuration revealed by the SEM and TEM images (see Figures 8 and 9 and Figure S2, Supporting Information), which is schematically represented in Figure 9b, produces the interesting volcano-shaped PEC property. At a Ag loading < 50% mole ratio, increasing the amount of Ag in the Ag–Fe<sub>2</sub>O<sub>3</sub> and Ag–Fe<sub>2</sub>O<sub>3</sub>(2%Sn) nanocomposites increases their photocurrent responses due to several reasons: (1) low Ag loading does not scatter or block significantly the incident light to nanocomposites; (2) well dispersed Ag nanoparticles have strong surface plasmon resonance (SPR)<sup>30</sup> near 400 nm, which might act as an efficient visible-light harvesting system for spectral sensitization of Fe<sub>2</sub>O<sub>3</sub>; (3) photo-electron–hole pair

(30) See, e.g., Kreibitz, U. In *Handbook of Optical Properties: Vol. II Optics of Small Particles, Interfaces, and Surfaces*; Hummel, R. E., Wibmann, P., Ed.; CRC Press: Boca Raton, 1997; Chapter 7.

separation at the Ag/semiconductor interface can be substantially enhanced by the high electric field near aggregates of Ag nanoparticles;<sup>31</sup> (4) electrons photogenerated at the Ag/Fe<sub>2</sub>O<sub>3</sub> interface away from the electrolyte solution can be effectively removed from the interface and transferred to well dispersed Ag nanoparticles and also Ag microparticle phase which serve as better three-dimensional percolation pathway and ohmic contact to the FTO substrate. This is consistent with the film resistance measurements in the dark (see Figure 12) and under irradiation (see Figure 10 for PEC measurements), suggesting that the films behave as a constant resistance device. However, as Ag content becomes higher (> 50% mole ratio) on the surface of Fe<sub>2</sub>O<sub>3</sub>, they overwhelmingly play important roles as a light-blocking medium and as recombination centers for photogenerated electrons and holes near the solid/electrolyte interface, and thus the photocurrent decreased with increasing Ag loading in this regime.

#### 4. Conclusion

We have shown with SPECM that addition of Ag improves the behavior of Fe<sub>2</sub>O<sub>3</sub> and that a Ag-Fe<sub>2</sub>O<sub>3</sub>(2%Sn)

(31) See, e.g., Catchpole, K.; Pillai, R. S. J. *Lumin.* **2006**, *121*, 315.

is even better, especially under visible light irradiation. Unlike a previously reported result, the content of Ag exceeded the usual amount for improvement of the Fe<sub>2</sub>O<sub>3</sub> photocatalyst, and the highest photocurrent was obtained at 1:1 Ag-Fe among different atomic ratios of Ag to Fe. Doping Sn into this material improved its photocurrent in 0.2 M NaOH under visible light irradiation ( $\lambda \geq 420$  nm). Ag-Fe<sub>2</sub>O<sub>3</sub>-(2%Sn) nanocomposite photocatalyst showed the highest photocurrent as well as good stability in alkaline solution (0.2 M NaOH) under UV and visible light irradiation. The IPCE of Ag-Fe<sub>2</sub>O<sub>3</sub>(2%Sn) obtained at 420 nm was 1.4 and 2.0% at 0.3 and 0.4 V vs Ag/AgCl, respectively.

**Acknowledgment.** Support from the Robert A. Welch Foundation, and the Korea Research Foundation #(F-0021) Grant funded by the Korean Government (MOEHRD) (KRF-2007-357-D00054) is gratefully acknowledged.

**Supporting Information Available:** Additional information as noted in text (PDF). This information is available free of charge via the Internet at <http://pubs.acs.org>.